

Supplementary Information

Zn(II)-nucleobase metal-organic nanofibers and nanoflowers: synthesis and photocatalytic application

*Bhagwati Sharma**^{a,b} *Arup Mahata,*^a *Sonam Mandani,*^{a,c} *Neha Thakur,*^a *Biswarup Pathak,*^a and
*Tridib K. Sarma**^{*,a}

^a*Discipline of Chemistry, Indian Institute of Technology Indore, Simrol, Khandwa Road, Indore-453552, India.*

^b*Department of Chemistry, Rewa Engineering College, Rewa, Madhya Pradesh-486002, India.*

^c*Present address: Department of Chemistry, Shri Govindram Seksaria Institute of Technology and Science, Indore-452003, India.*

Email: bhagu18.2008@gmail.com; tridib@iiti.ac.in

DFT Studies

DFT calculations were performed using Gaussian 09 program¹ using M062X level of theory as this functional incorporates the dispersion interaction more accurately for non-bonded interactions.² We have used 6-311++G** basis set for the main group atoms and DGDZVP for the Zinc atom. The effects of the water solvation on the structures and relative energy of the complexes are taken into account by means of the polarizable continuum model (PCM).³⁻⁷ Binding energies are calculated as the difference between the electronic energy of the complexes and the respective monomers, i.e.

$$\Delta E = E_{N-Ag} - (E_N + E_{Ag})$$

where E_{N-Ag} is the total energy of the nucleobase-Zinc complex, E_N , and E_{Ag} are the energies of the nucleobases and zinc ion, respectively.

Here, N9-H, N1-H, N1-H, N3-H and N3-H are the most acidic hydrogen atoms of adenine, guanine, cytosine, uracil, and thymine, respectively. The Zn-(nucleobase) structures are modelled by considering a mono-negatively charged nucleobase binding with a divalent Zn(II) ion. Thus, the overall charge of the complex is +1. The Zn-(nucleobase)₂ structures are modelled by considering the binding of two negatively charged nucleobases with a divalent Zn(II) ion. Here, the system is a neutral one.

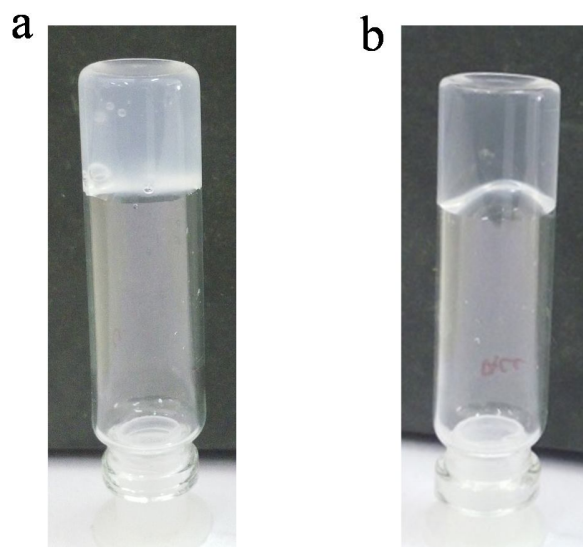


Figure S1. Digital images of Zn-cytosine hydrogel formed using alkaline cytosine and (a) ZnCl_2 and (b) $\text{Zn}(\text{CH}_3\text{COO})_2$.

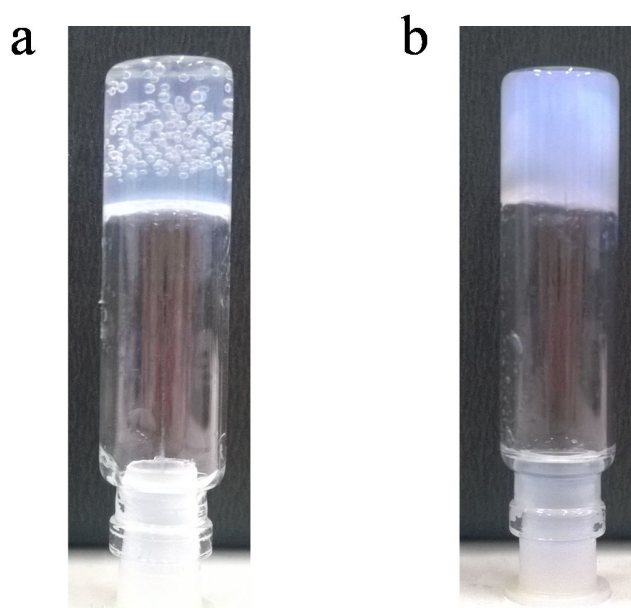


Figure S2. Digital images of the Zn-cytosine gels formed in (a) methanol- H_2O mixture and (b) pure methanol.

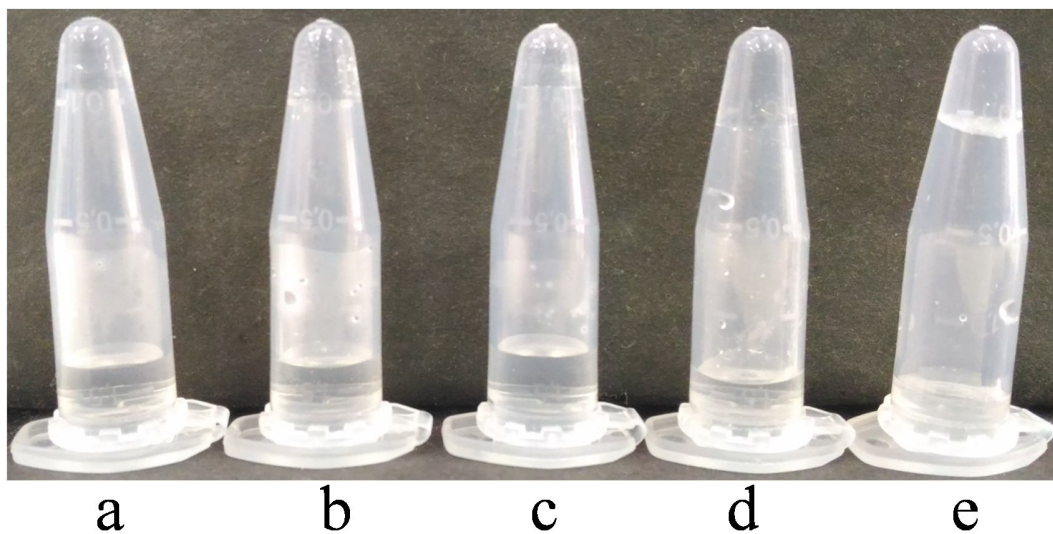


Figure S3. Digital images of the clear solutions obtained upon the addition of $\text{Zn}(\text{NO}_3)_2$ to an acidic solution of (a) adenine, (b) guanine, (c) cytosine, (d) thymine and (e) uracil.

Cytosine (M)	Zn^{2+} (M)	Result
0.2	0.2	Gel
0.2	0.15	Gel
0.2	0.1	Weak Gel
0.2	0.05	Very weak gel, turns into sol on slight shaking
0.15	0.2	Gel
0.1	0.2	Weak Gel
0.05	0.2	Very weak gel, turns into sol on slight shaking

Table S1. Supramolecular structures formed by the interaction of cytosine and Zn^{2+} ions at various Zn^{2+} :cytosine molar concentrations.

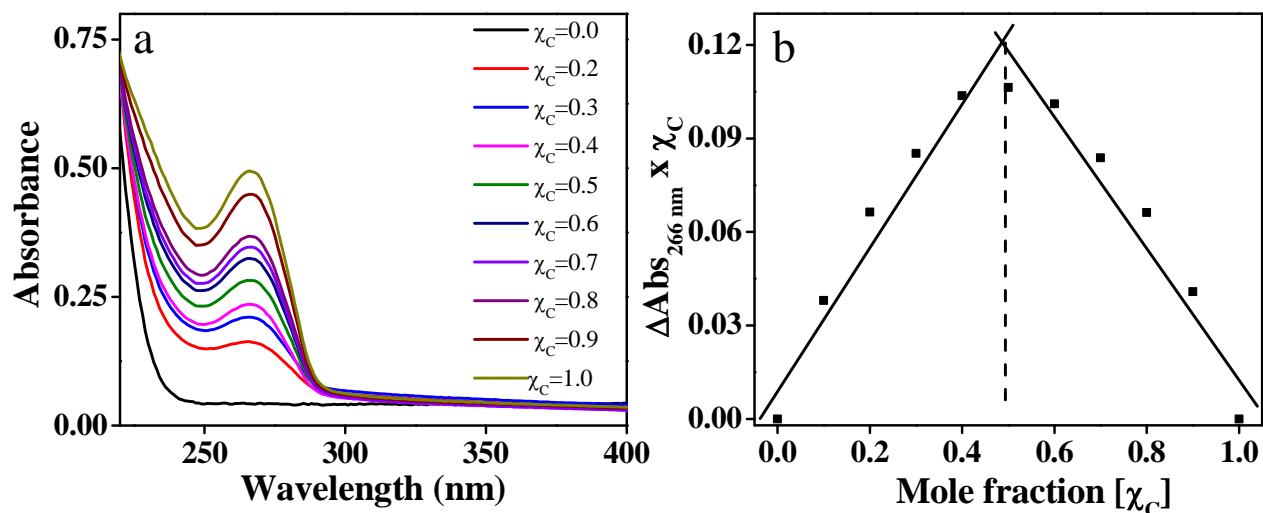


Figure S4. UV-visible spectra of Zn-C complex formed at varying mole fractions of cytosine and (b) Job's plot constructed by observing the changes in absorbance at 266 nm upon addition of varying mole fractions of cytosine to aqueous $\text{Zn}(\text{NO}_3)_2$ solution.

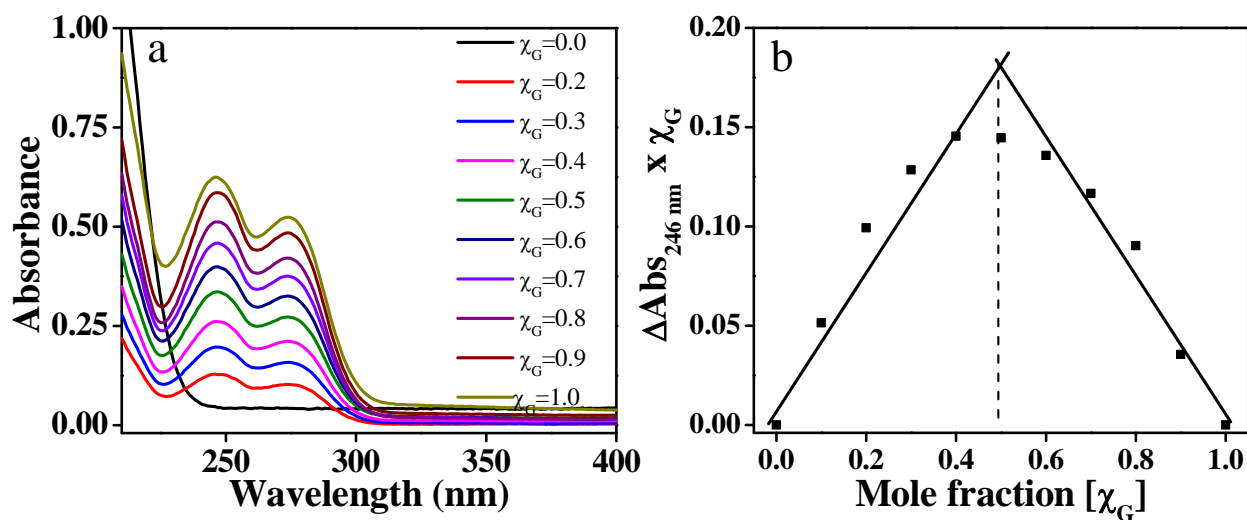


Figure S5. UV-visible spectra of Zn-G complex formed at varying mole fractions of guanine and (b) Job's plot constructed by observing the changes in absorbance at 246 nm upon addition of varying mole fractions of guanine to aqueous $\text{Zn}(\text{NO}_3)_2$ solution.

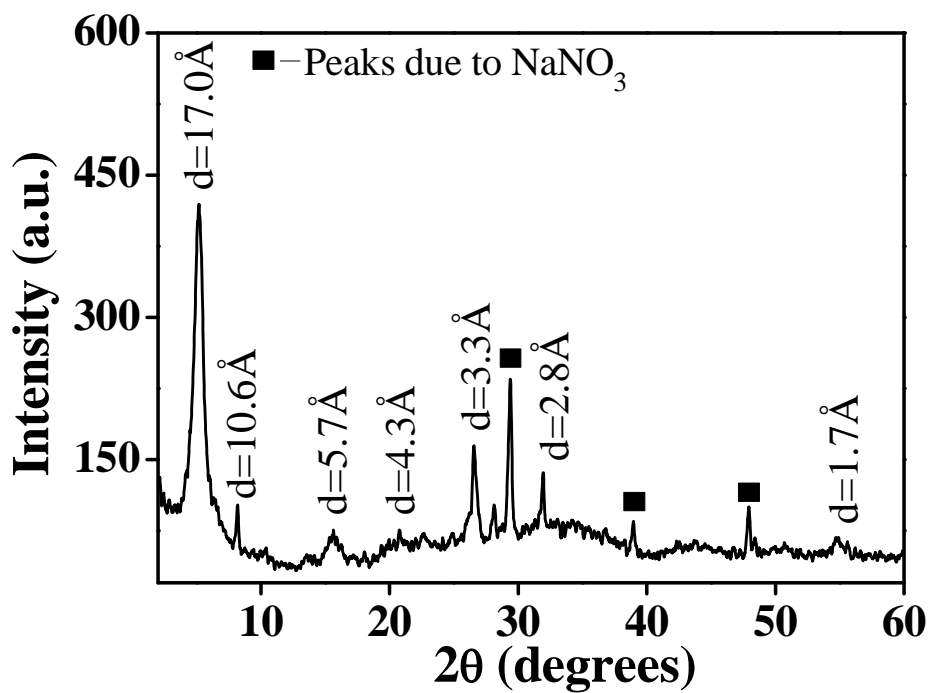


Figure S6. Powder XRD pattern of the Zn-C hydrogel showing the peaks with the corresponding d -values.

The powder XRD pattern for the lyophilized Zn-C gel showed well resolved diffraction peaks which indicate that the hydrogel was crystalline in nature.

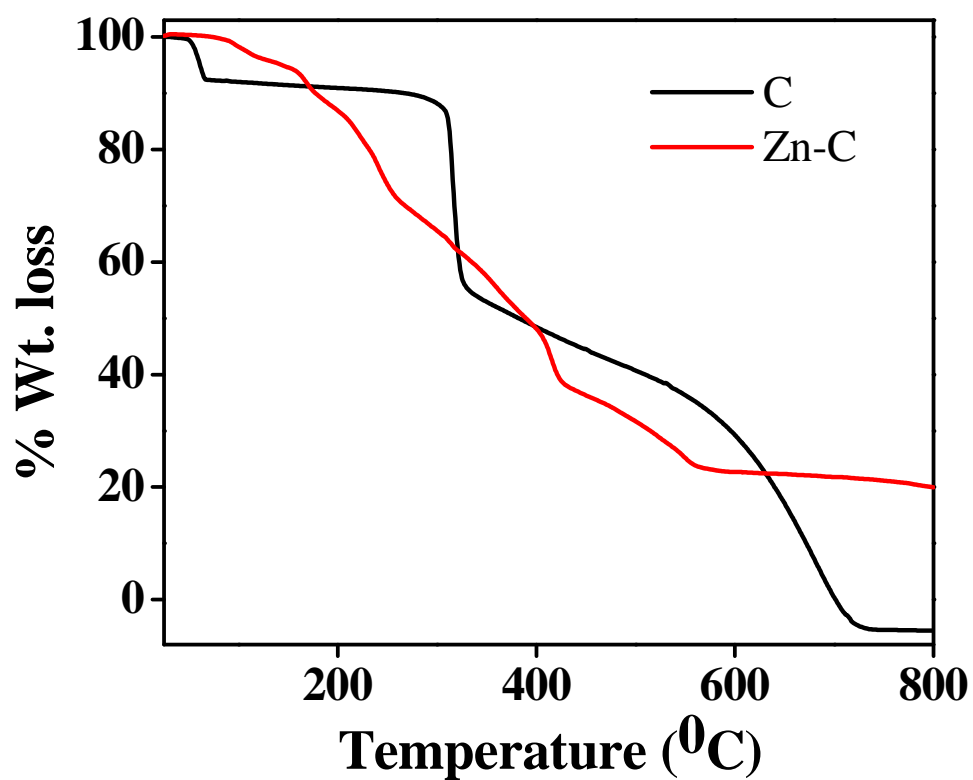


Figure S7. TGA plot of the pure cytosine and lyophilized Zn-cytosine xerogel.

The TGA plot for pure cytosine showed three weight losses at 55 °C, 305 °C and 510 °C resulting in complete decomposition of the organic components. In the TGA plot of Zn-C, similar weight losses were observed. The material however, was stable beyond 720 °C, with a composition of 23%, which might be due to the stability of the metal.

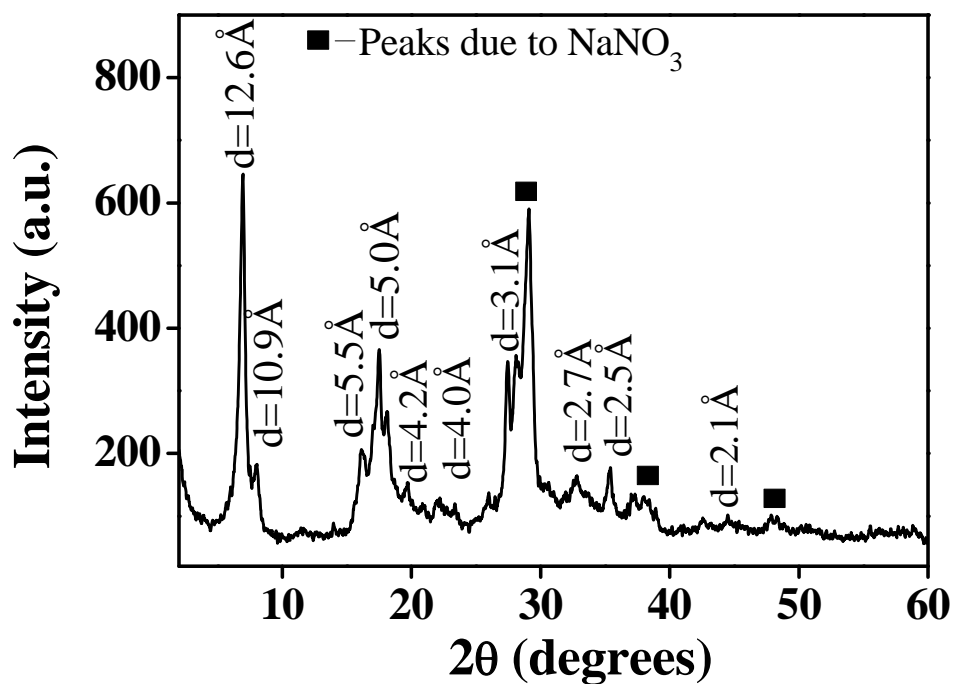


Figure S8. Powder XRD pattern of the Zn-G hydrogel showing crystalline peaks with the corresponding d -values.

The powder XRD pattern for the lyophilized Zn-G gel showed well resolved diffraction peaks which indicate that the hydrogel was crystalline in nature.

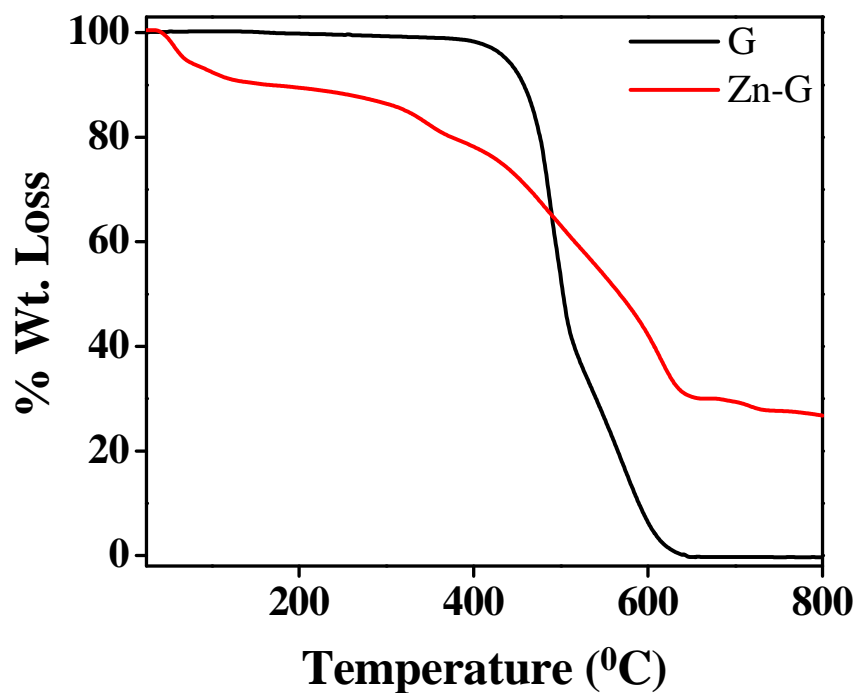


Figure S9. TGA plot of pure guanine and lyophilized Zn-G xerogel.

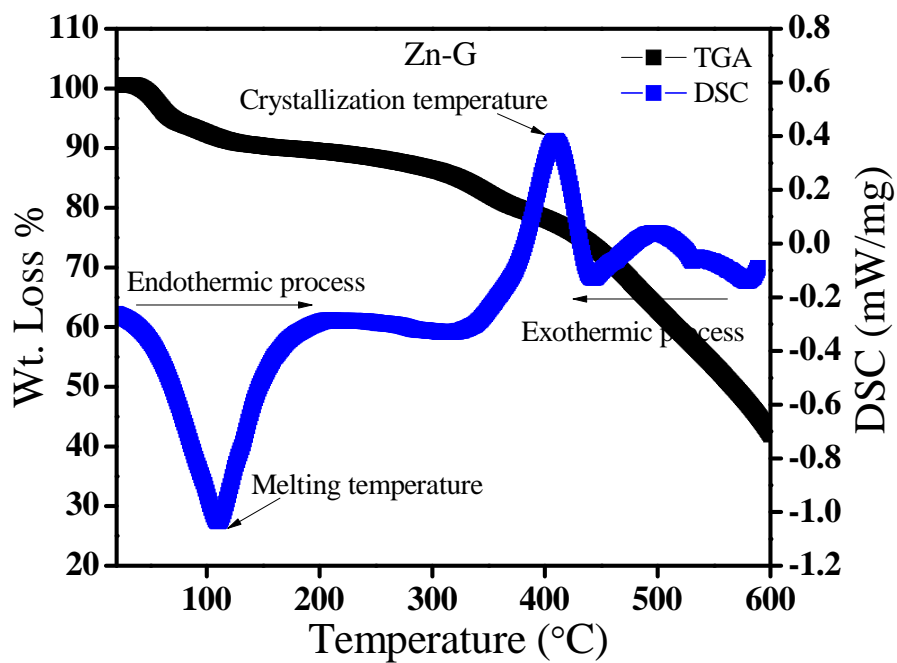


Figure S10. TGA and DSC plot of lyophilized Zn-G xerogel.

The TGA plot of guanine (G) showed two pronounced steps of weight loss, a sharp step with approximately 60% weight loss in the temperature range of 410–520 °C and a further weight loss of approximately 36 wt% from 520 to 640 °C. In this process, guanine was completely decomposed. On the other hand, Zn-G composite shows a completely different pattern in the TG plot, with approximately 8% weight loss at 100-110 °C, and a gentle weight loss of 7% in the range of 120-280 °C. Further weight loss of 21 wt% was observed in the range of 380-460 °C. Finally, a weight loss of 35% was observed in the range of 450-630 °C with 29% of residue left.

From the DSC plot of the Zn-G xerogel, an endothermic peak at 110 °C was observed, which could be assigned to the release of water of crystallization. A prominent exothermic peak at 420 °C, could be attributed to the release of guanine ligand from the Zn-G complex and subsequent formation of ZnO.

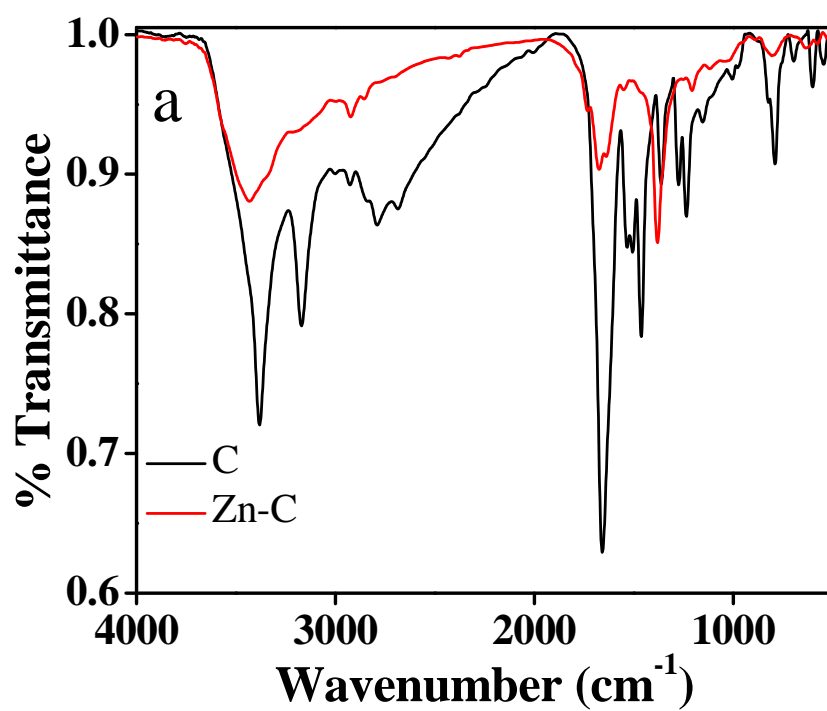


Figure S11. FTIR spectrum of (a) pure cytosine and Zn-cytosine.

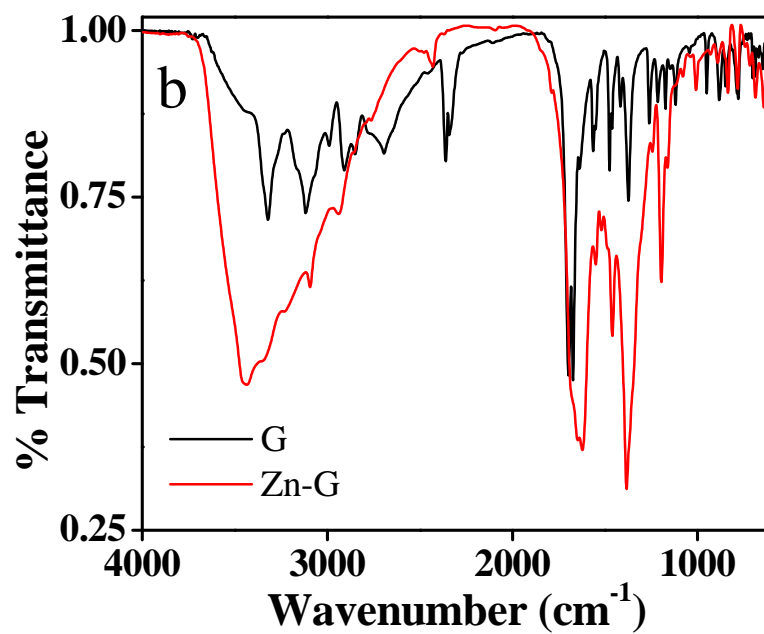


Figure S12. FTIR spectrum of (a) pure guanine and Zn-guanine.

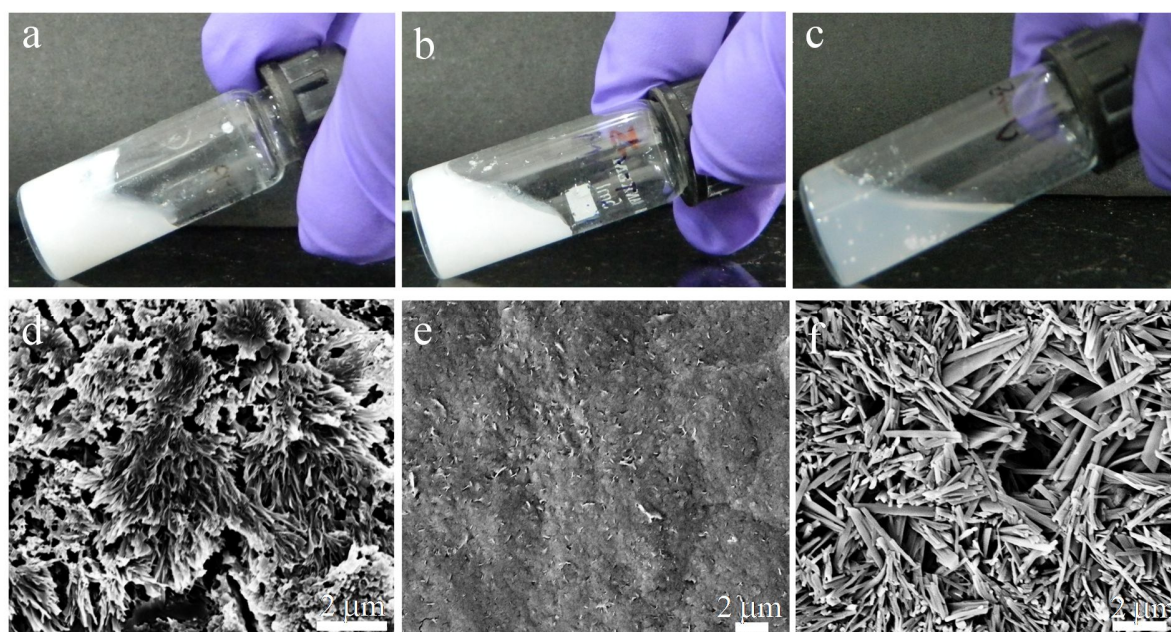


Figure S13. (a), (b) and (c) Digital images of the precipitate formed upon the addition of $\text{Zn}(\text{NO}_3)_2$ to an alkaline solution of adenine, thymine and uracil respectively. (d), (e) and (f) FESEM images of the Zn-A, Zn-T and Zn-U precipitates respectively.

Relative Energy (kcal/mol)									
Adenine		Guanine		Uracil		Cytosine		Thymine	
N1	9.28	N7-O	0.00	N1	1.00	N1-O	0.00	N1	1.05
N3	4.58	N1-O	0.51	N3	0.00	N3-O	1.60	N3	0.00
N7	3.14	N3-N9	13.30	N1-O	1.56	-	-	N1-O	1.92
N9	0.00	-	-	N3-O	0.06	-	-	N3-O	1.63
N3-N9	6.86	-	-	-	-	-	-	-	-

Table S2. Relative energies for the binding of Zn^{+2} ions at different sites of adenine, guanine, uracil, cytosine and thymine.

Formation Energy (kcal/mol)					
Zn-nucleobase	Adenine	Guanine	Uracil	Cytosine	Thymine
Zn-(nucleobase)	-48.08	-55.26	-52.58	-56.86	-52.31
Zn-(nucleobase) ₂	-98.95	-108.89	-105.70	-112.32	-105.93

Table S3. Formation energies for the Zn-(nucleobase) and Zn-(nucleobase)₂ unit.

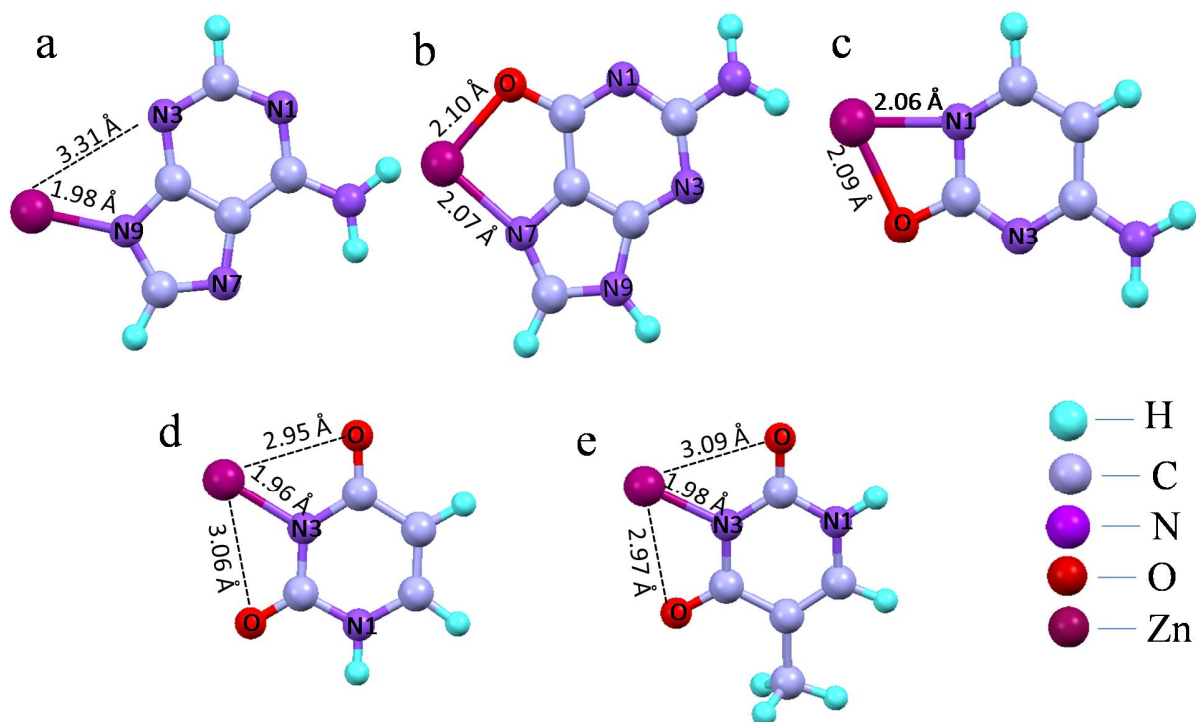


Figure S14. Optimized structures of mono-cationic Zn(II)-nucleobases in basic medium: (a) Zn-adenine, (b) Zn-guanine, (c) Zn-cytosine, (d) Zn-uracil and (e) Zn-thymine.

	% C
[Zn(C)(H ₂ O) ₃] calculated	21.09
[Zn(C) ₂ (H ₂ O) ₂] calculated	30.04
Experimental	21.00

Table S4. Elemental analysis with respect to % of Carbon in the Zn-cytosine complex calculated theoretically and experimentally.

	% C
[Zn(G)(H ₂ O) ₃] calculated	22.43
[Zn(G) ₂ (H ₂ O) ₂] calculated	30.03
Experimental	20.37

Table S5. Elemental analysis with respect to % of Carbon in the Zn-guanine complex calculated theoretically and experimentally.

As can be seen from the tables, the % of carbon in case of both Zn-C and Zn-G is more than the % of carbon theoretically calculated in Zn-(nucleobase) complex. In the gels, there are excess of other elements like N, O, H and Na from nitrate and hydroxide which have not been accounted for while calculation of % of C in Zn-C or Zn-G complexes. In such a scenario, the actual % of C will be less than the theoretical calculations. Therefore, we can conclude that Zn²⁺ forms Zn-(nucleobase) complexes, which is consistent with Job's plot result.

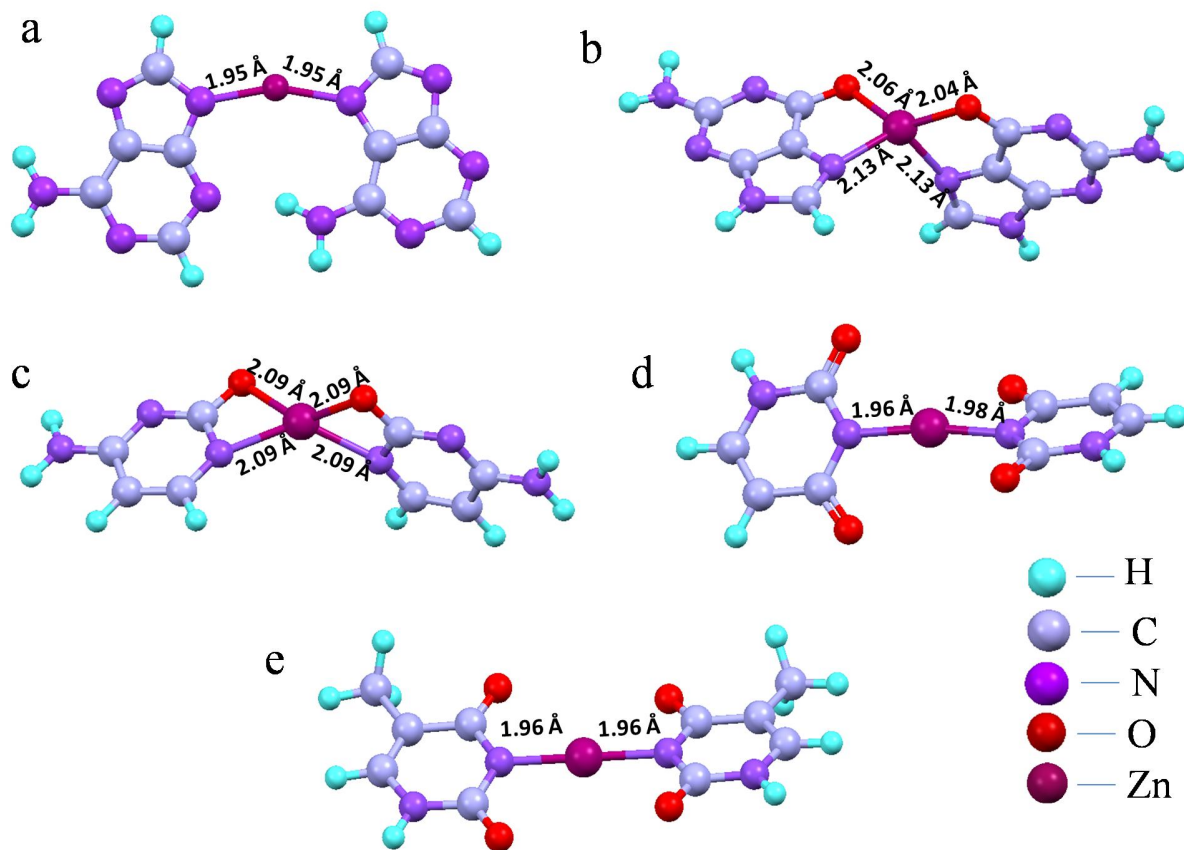


Figure S15. Optimized structures of neutral Zn(II)-(nucleobase)₂ in basic medium: (a) Zn-(adenine)₂, (b) Zn-(guanine)₂, (c) Zn-(cytosine)₂ (d) Zn-(uracil)₂ and (e) Zn-(thymine)₂.



Figure S16. Digital image of the precipitate formed upon addition of $\text{Zn}(\text{NO}_3)_2$ to a mixture of cytosine and guanine.

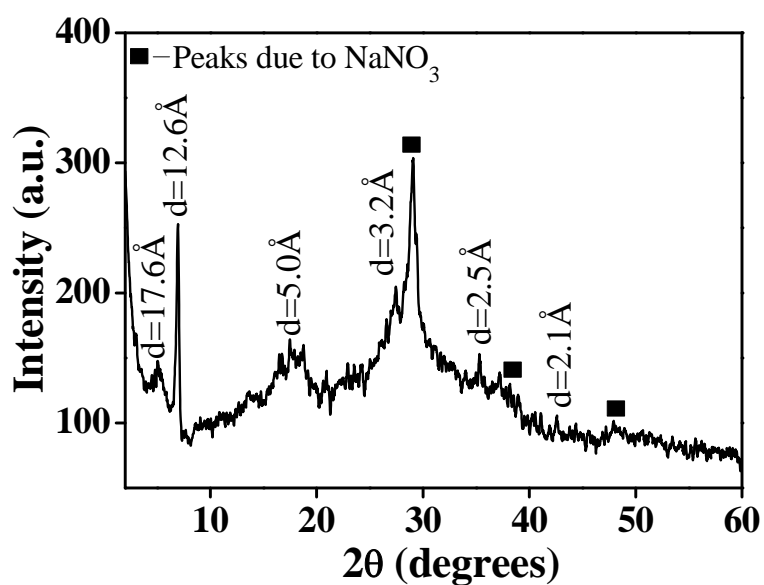


Figure S17. Powder XRD pattern of the Zn-C-G precipitate.

The crystalline nature of the Zn-C-G precipitate composed of nanoflowers could be established from the powder XRD studies. The powder XRD pattern of the nanoflowers showed multiple peaks in 2θ range between 2 to 60 degrees.

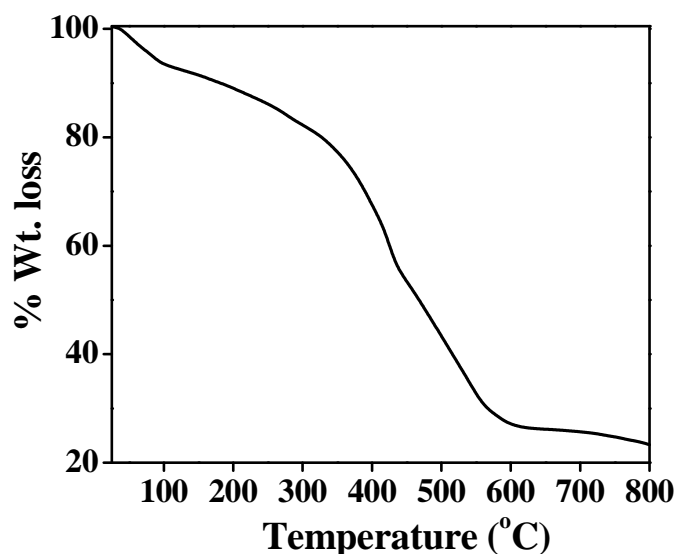


Figure S18. TGA plot of the Zn-C-G precipitate.

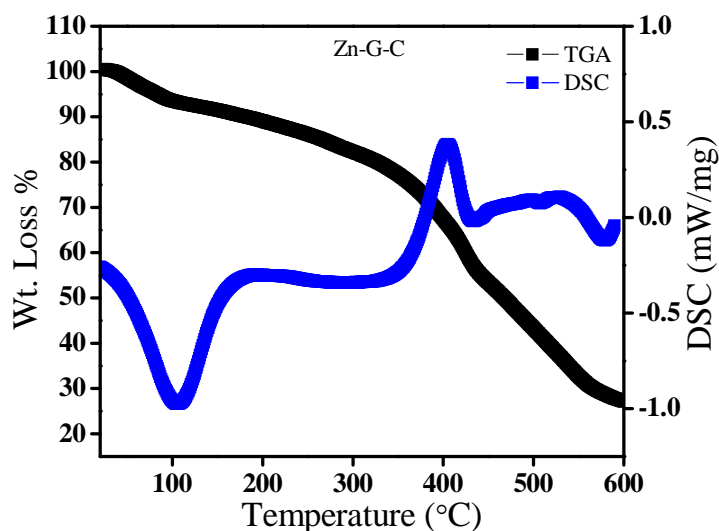


Figure S19. TGA and DSC plot of the Zn-C-G precipitate

The thermal stability of the nanoflowers was studied by thermogravimetric analysis, which initially showed a loss of 7.5% at 115 °C corresponding to the loss of water molecules. Then another weight loss upto 600 °C was observed, which can be attributed to the decomposition of the ligands in the complex. The DSC plot of the Zn-C-G precipitates showed an endothermic peak at 110 °C, corresponding to the release of water molecules and an exothermic peak at 408 °C, which could be attributed to the dissociation of the nucleobases from the complex.

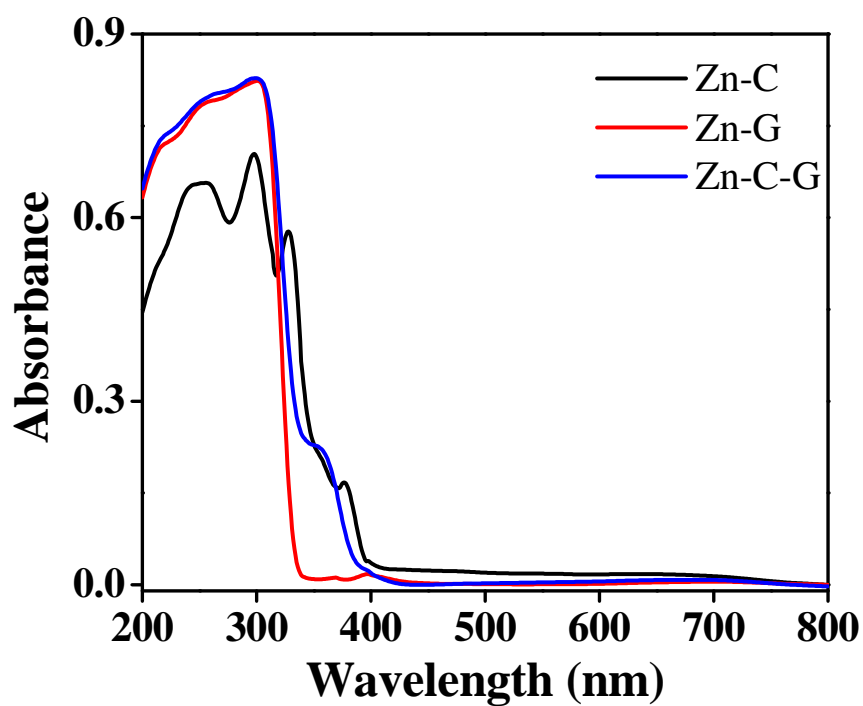


Figure S20. Solid state UV-visible spectrum for the calculation of the band gap of the three Zn based materials.

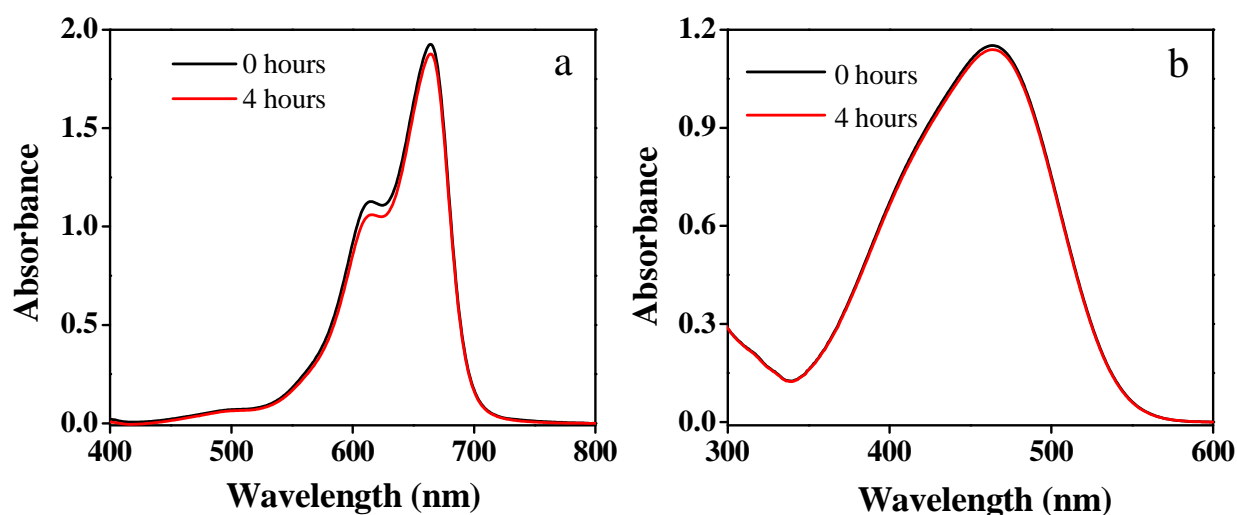


Figure S21. Control experiment carried out in the absence of light for the degradation of (a) MB and (b) MO, showing no obvious changes in the UV-visible spectrum.

Photocatalytic studies:

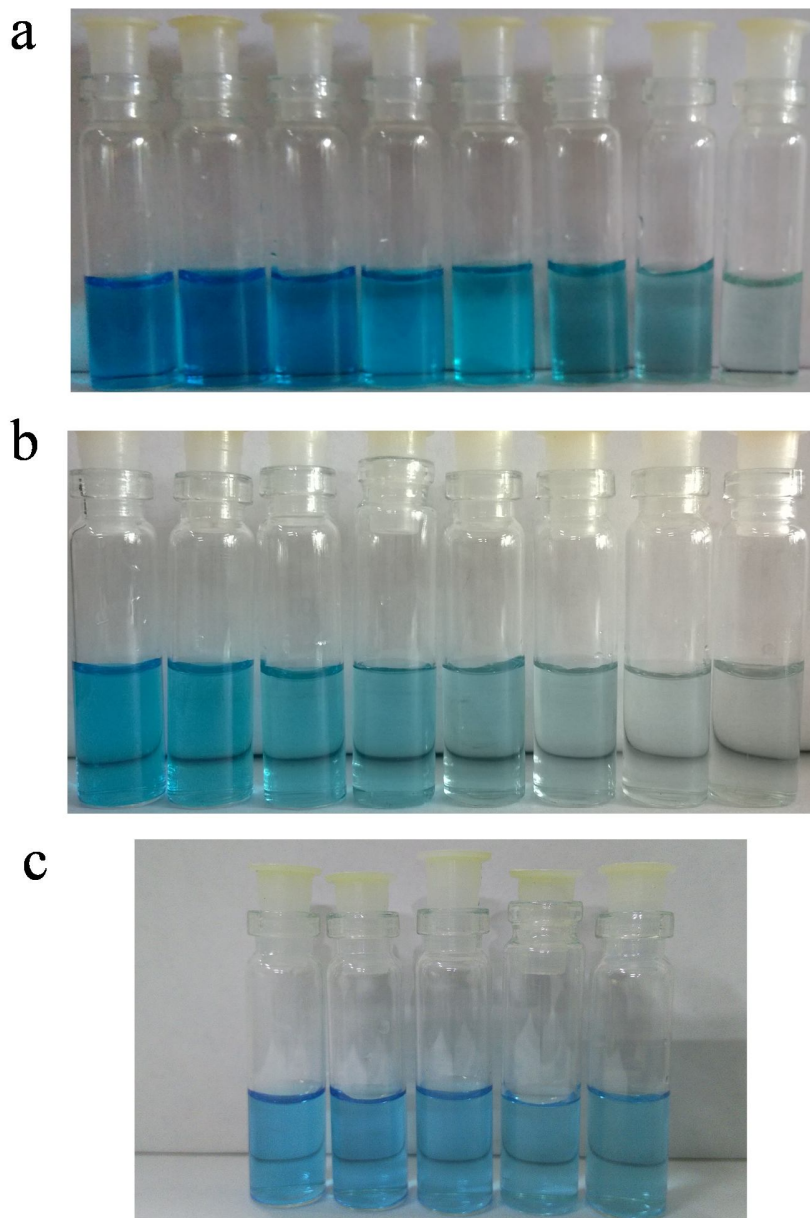


Figure S22. Digital images showing the degradation of methylene blue using the three materials as catalysts, (a) Zn-cytosine at an interval of 10 mins, (b) Zn-guanine at an interval of 10 mins and (c) Zn-cytosine-guanine at an interval of 20 mins.

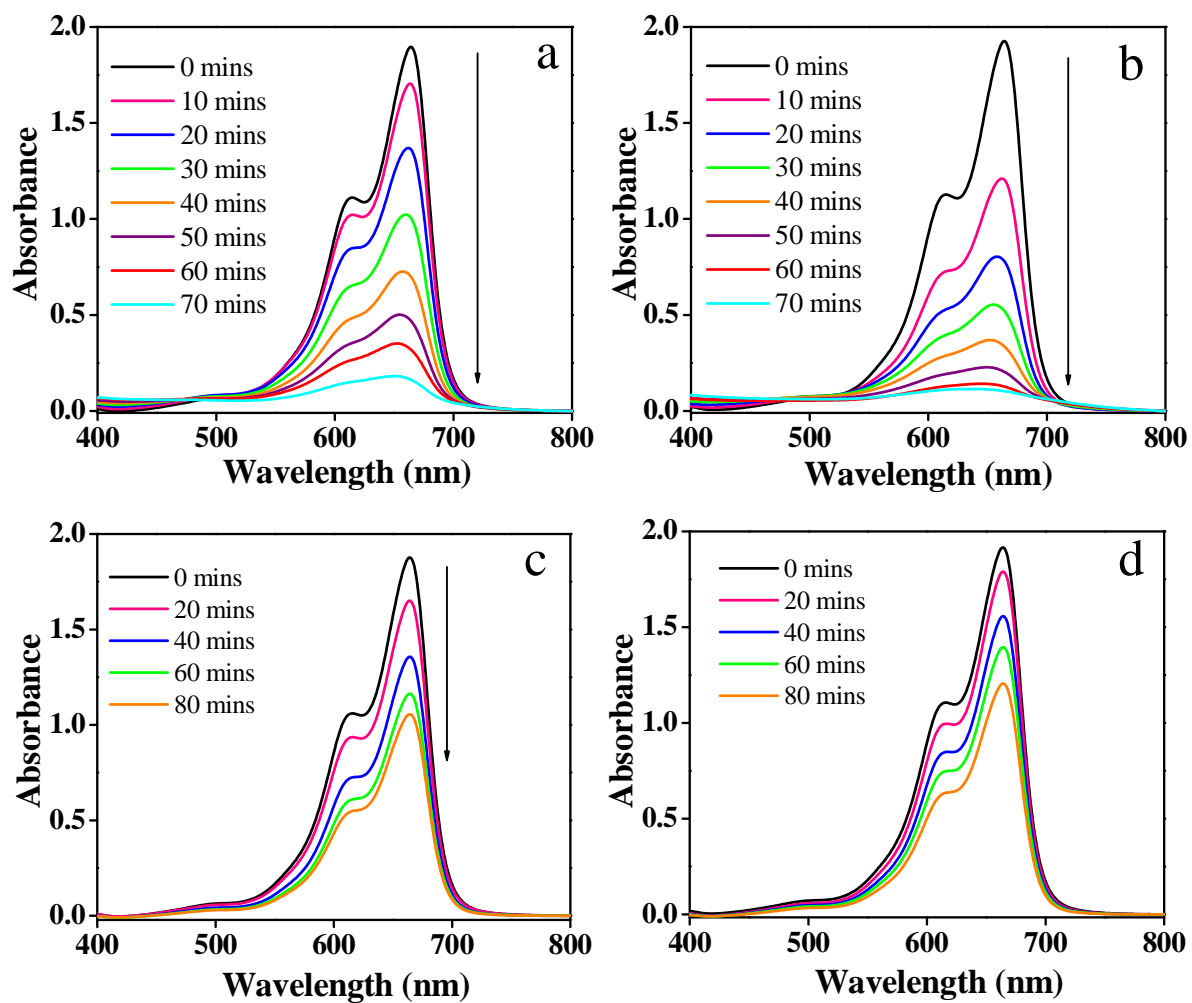


Figure S23. Time dependent UV-visible spectra for the degradation of methylene blue using the three Zn based materials as catalysts, (a) Zn-cytosine, (b) Zn-guanine, (c) Zn-cytosine-guanine and (d) blank (without any catalyst).

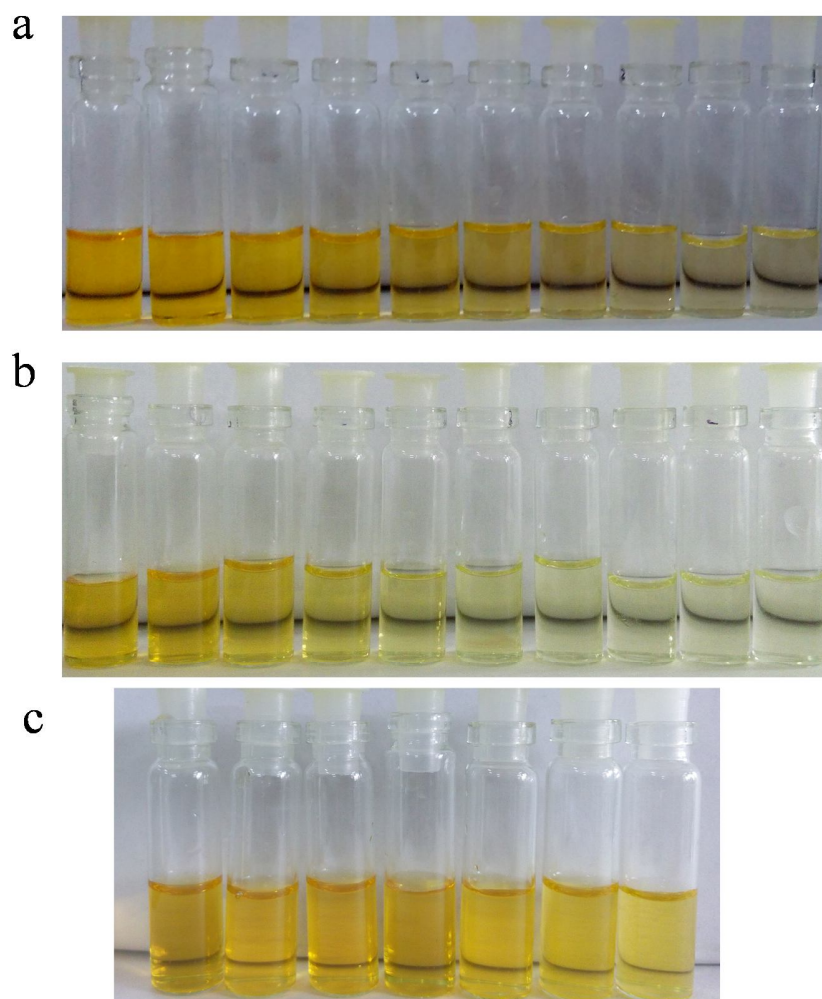


Figure S24. Digital images showing the degradation of methyl orange with the three catalysts, (a) Zn-cytosine at an interval of 10 mins, (b) Zn-guanine at an interval of 10 mins and (c) Zn-cytosine-guanine at an interval of 15 mins.

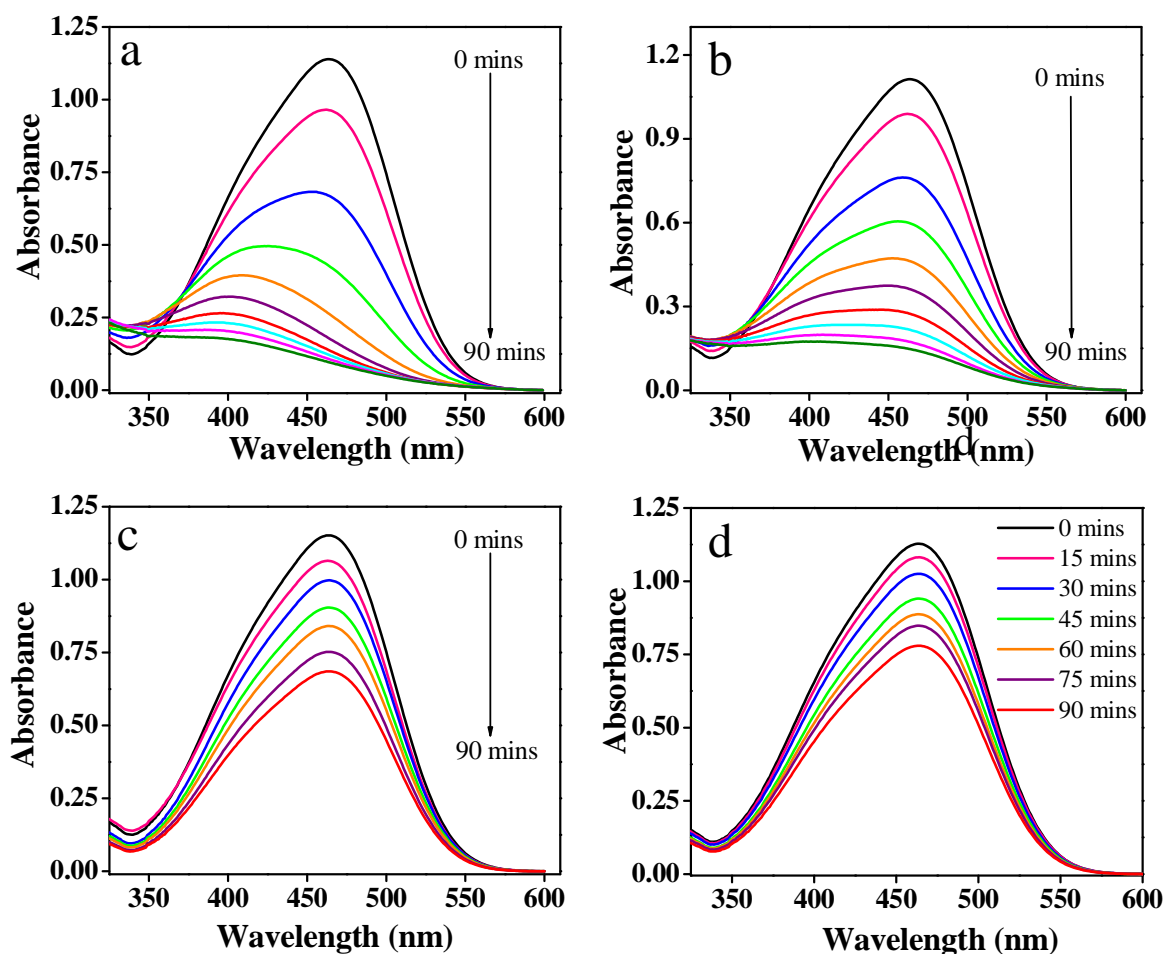


Figure S25. Time dependent UV-visible spectra for the degradation of methyl orange using the three Zn based materials as catalysts, (a) Zn-cytosine, (b) Zn-guanine, (c) Zn-cytosine-guanine and (d) blank (without any catalyst).

The photocatalytic degradation of methyl orange with the three Zn-based catalysts was carried out with a dye concentration of 15 mg/L. From the time dependent UV-visible studies, it was observed that the illumination of the dye solution containing the catalysts with a UV lamp led to a decrease in intensity of the peak at 464 nm due to MO with time. It was found that whereas Zn-C nanofibers degraded 84% of MO in 90 minutes, the use of Zn-G nanofibers as catalyst afforded the degradation of methyl orange by 86% under similar duration of time. On the other hand, the flower shaped coordination polymer particles could degrade the dye only by 43% in 90 minutes.

Photocatalytic mechanism

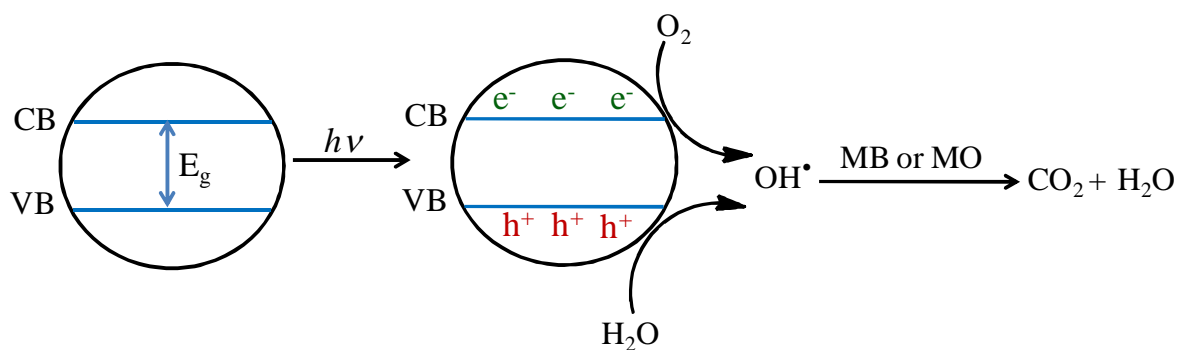
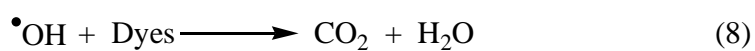
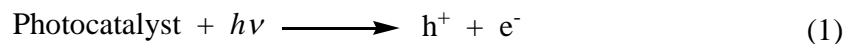


Figure S26. Schematic representation of the photocatalytic degradation of organic pollutant dyes by Zn-C and Zn-G nanofibers as well as Zn-C-G nanoflower photocatalysts.

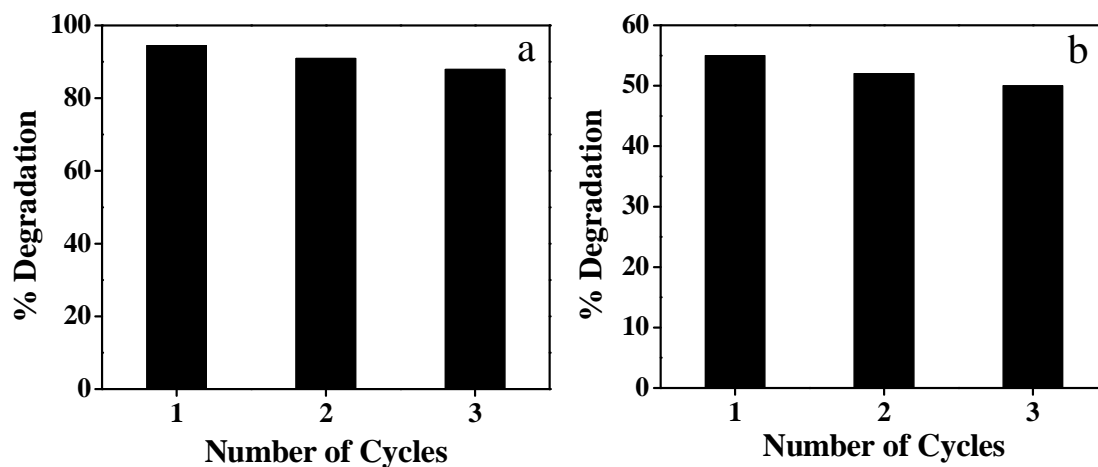


Figure S27. (a) Recyclability studies of (a) Zn-G and (b) Zn-C-G photocatalyst for the photocatalytic degradation of methylene blue in three successive cycles.

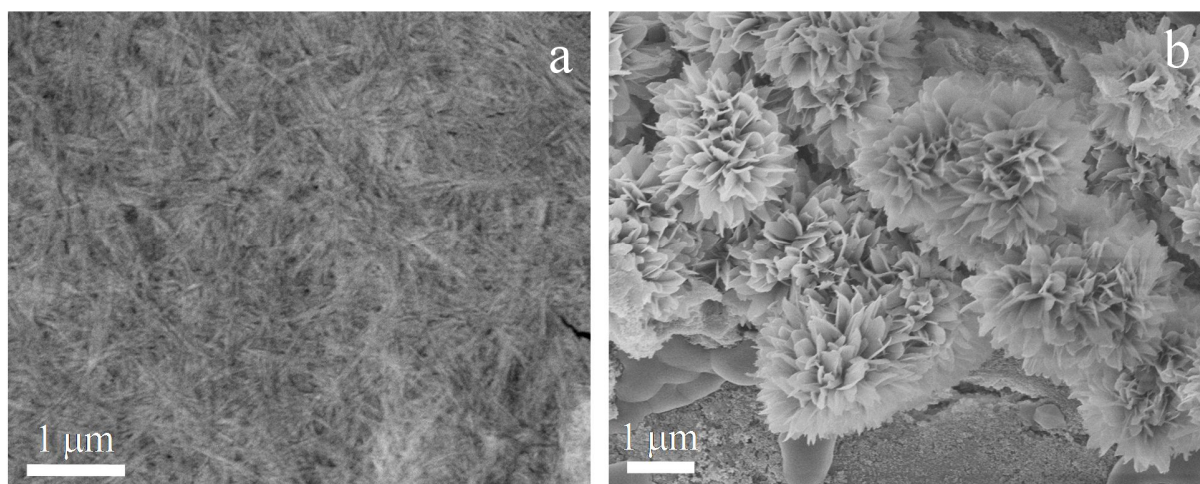


Figure S28. (a) SEM image of the Zn-G photocatalyst showing the retention of the nanofibrous morphology even after the third catalytic cycle. (b) SEM image of the Zn-C-G catalyst showing the presence of coordination polymer nanoflowers after third cycle of reaction.

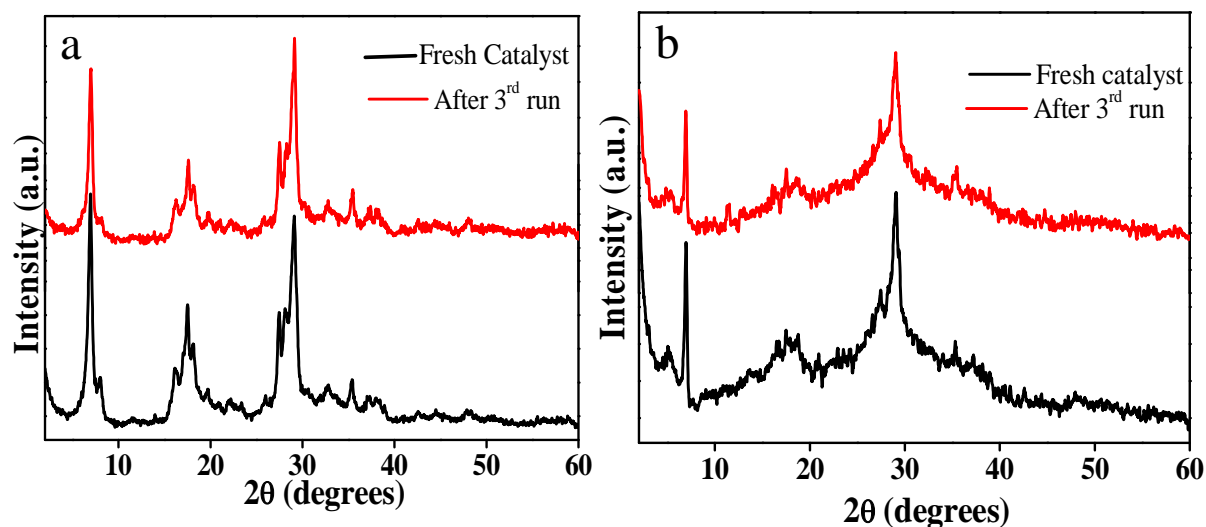


Figure S29. (a) Comparison of the powder X-ray pattern of fresh Zn-G photocatalyst and catalyst after three runs. (b) Comparison of the powder X-ray pattern of fresh Zn-C-G photocatalyst and catalyst after three successive runs.

References

1. Frisch, M. J. *et al.* Gaussian 09, Revision A.1, Gaussian, Inc., Wallingford CT, 2009.
2. Zhao, Y.; Truhlar, D. G. Density Functionals with Broad Applicability in Chemistry. *Acc. Chem. Res.* **2008**, *41*, 157-167.
3. Tomasi, J.; Persico, M. Molecular Interactions in Solution: An Overview of Methods Based on Continuous Distributions of the Solvent. *Chem. Rev.* **1994**, *94*, 2027-2094.
4. Cossi, M.; Barone, V.; Cammi, R.; Tomasi, J. Ab Initio Study of Solvated Molecules: A New Implementation of the Polarizable Continuum Model. *Chem. Phys. Lett.* **1996**, *255*, 327-335.
5. Barone, V.; Cossi, M.; Tomasi, J. A New Definition of Cavities for the Computation of Solvation Free Energies by the Polarizable Continuum Model. *J. Chem. Phys.* **1997**, *107*, 3210-3221.
6. Barone, V.; Cossi, M.; Tomasi, J. Geometry Optimization of Molecular Structures in Solution by the Polarizable Continuum Model. *J. Comput. Chem.* **1998**, *19*, 404-417.
7. Cossi, M.; Barone, V. Analytical Second Derivatives of the Free Energy in Solution by Polarizable Continuum Models. *J. Chem. Phys.* **1998**, *109*, 6246-6254.